

Morphotropic Phase boundary in BNT-BZT solid solution: A study by Raman spectroscopy and electromechanical parameters

B. Parija^a, T. Badapanda^{b*} and S. Panigrahi^c

^aGovt. (Auto) college, Rourkela, Odisha -769004 India

^bDepartment of Physics, C V Raman College Engineering, Bhubaneswar, Odisha, India

^cDepartment of Physics, National Institute of Tehnology, Rourkela, Orissa, India

Lead-free perovskite ferroelectric ceramics of $(1-x)(\text{Bi}_{0.5}\text{Na}_{0.5})\text{TiO}_3-x \text{Ba}(\text{Zr}_{0.25}\text{Ti}_{0.75})\text{O}_3$ [abbreviated as $(1-x)\text{BNT}-x\text{BZT}$] have been synthesized via conventional solid-state reaction route. Structural changes of the solid-solutions were investigated by using rietveld refinement of X-ray diffraction (XRD) data and Raman spectroscopy over the composition range $0 \leq x \leq 0.08$. The unique phase transition behaviours are discussed in relation to the growth of $\text{Ba}^{2+}\text{TiO}_3$ and $\text{Zr}^{4+}\text{TiO}_3$ clusters upon the substitution of Ba^{2+} for $(\text{Bi}_{0.5}\text{Na}_{0.5})^{2+}$ cations and Zr^{4+} for Ti^{4+} in the $(1-x)\text{BNT}-x\text{BZT}$ solid-solutions. The splitting of (111) and (200) plane represents the presence of morphotropic phase boundary within the solid solution at $x = 0.05$. Raman spectroscopy exhibited a splitting of the (TO3) mode at $x = 0.05$ and confirmed the presence of MPB region. The piezoelectric properties of the solid solution increase with rise in $\text{Ba}(\text{Zr}_{0.25}\text{Ti}_{0.75})\text{O}_3$ content and shows optimum value at $x = 0.05$ owing to the co-existence of two ferroelectric phases. Based on these results, it is suggested that the morphotropic phase boundary in the studied system lies in the composition $x = 0.05$.

Key words: $(\text{Bi}_{0.5}\text{Na}_{0.5})\text{TiO}_3$; $\text{Ba}(\text{Zr}_{0.25}\text{Ti}_{0.75})\text{O}_3$, Solid-solutions, Morphotropic Phase boundary, Reitveld refinement, Raman spectroscopy, electromechanical properties.

Introduction

Structure-property relationships are an important aspect in material physics as the knowledge of these can be utilized to develop novel materials with improved qualities. Perovskite-based ferroelectric and piezoelectric materials have been at the center of research because their simple structure facilitates the understanding of the structure property relationships. Among the perovskites, $\text{Bi}_{0.5}\text{Na}_{0.5}\text{TiO}_3$ ceramic with a rhombohedral structure has been considered to be a good candidate for lead-free piezoelectric ceramics because of its strong ferroelectric nature at room temperature, high Curie temperature ($T_c = 320^\circ\text{C}$), relatively larger remnant polarization ($P_r = 38 \mu\text{C}/\text{cm}^2$), and coercive field of $E_c = 73 \text{ kV}/\text{cm}$ at room temperature [1]. In BNT, the bismuth and sodium cations occupy the corners of a cubic unit cell, oxygen cations occupying the face centers forming an octahedral and a titanium cation in the center of the oxygen octahedra. BNT is one among the few A-site disorder perovskite material, having a mixture of Bi^{3+} and Na^{1+} ions. BNT is a perovskite-structured ferroelectric with a rhombohedral symmetry ($R3c$) at

RT. The crystal structure changes to the tetragonal ($P4bm$) and then to the cubic ($Pm3m$) structure at approximately 300 and 540°C , respectively, upon heating [2-6].

In recent years, lead-free perovskite ceramics have attracted considerable attentions as one of the important materials because of its outstanding advantages in free control atmosphere and no lead pollution. The intriguing phase transitions of both BNT and BNT-based solid solutions as a function of composition and temperature make them an excellent model for studies on the phase transition behaviours of relaxor ferroelectrics [7-10]. BNT ceramic is difficult due to its high conductivity. Furthermore, the piezoelectric properties of BNT ceramic are too low to be for practical application. In order to improve the poling process and then obtain good piezoelectric properties, some modification or doping of the BNT system has been carried out. It has been reported that BNT-based ceramics with their compositions modified with the addition of various ceramic oxides make it easier to be poled compared with pure BNT ceramics and improved piezoelectric properties [11-17]. The other feature of BNT is that it forms a morphotropic phase boundary (MPB) with other perovskites having tetragonal symmetry such as BaTiO_3 and $\text{Bi}_{1/2}\text{K}_{1/2}\text{TiO}_3$, and very strong piezoelectric properties are obtained for the MPB compositions [17-31]. Thus, BNT-based solid solutions have attracted much attention as lead-free piezoelectric materials.

*Corresponding author:
Tel : +91-9437306100
Fax: +91-674 2462022
E-mail: badapanda.tanmaya@gmail.com

Most studies on BNT-based solid solutions have focused on the MPB composition suitable for actuator applications. Among, the solid solutions, the solid solution with BT has been shown to have enhanced physical properties corresponding to a rhombohedral-tetragonal morphotropic phase boundary (MPB) [32]. Ba(Zr_{1-x}Ti_x)O₃ (BZT) ceramics also have received much attention for its excellent dielectric properties [33-36]. In the present work, ZrO₂ has been added into the B site of the perovskite BNBT ceramics in order to enhance the piezoelectric properties. There are very few reports available on the BNT-BZT solid solutions [37-40]. The present composition is chosen because Ba(Zr_{0.25}Ti_{0.75})O₃ (BZT) is an important B-site complex perovskite-type cubic structure with space group (Pm3m) and relaxor ferroelectric in nature. The detailed structural and dielectric study was already reported by the authors [41]. In recent years, Raman spectroscopy has been widely used for studying structural phase transitions in piezoelectric systems exhibiting MPBs. The present study reports the X-Ray diffraction, Raman scattering studies and electromechanical properties of BNT-BZT solid solution with a special emphasis on searching for the MPB.

Experiment

The samples were prepared by a conventional mixed oxide process. In the first step (Bi_{0.5}Na_{0.5})TiO₃ (BNT) and Ba(Zr_{0.25}Ti_{0.75})O₃ (BZT) master batches were made from Barium Carbonate-BaCO₃ (reagent grade Meark, India), Zirconium Oxide-ZrO₂ (reagent grade, Loba chem.), Titanium Oxide-TiO₂ (reagent grade, Merck), Bismuth Oxide-Bi₂O₃ (reagent grade Meark, India) and Sodium Carbonate-Na₂CO₃ (reagent grade, Merck). All the precursors are having purity of 99.9%. Appropriate amount of reagents were mixed in a zirconia media for 12 hrs using a laboratory designed ball milling unit. The BNT sample was calcined at 700 °C for 4 hrs and at 850 °C for 4 hrs with intermediate grinding and mixing. The BZT sample was calcined at 1000 °C for 4 hrs and at 1250 °C for 4 hrs with intermediate grinding and mixing. The phase purity of both the master samples was investigated using X-ray diffraction (XRD), (Xpert MPD, Philips, UK). Appropriate amount of BNT and BZT were mixed thoroughly to obtain (1-x)(Bi_{0.5}Na_{0.5})TiO₃-xBa(Zr_{0.25}Ti_{0.75})O₃ (abbreviated as BNT-BZT hereafter) solid-solution. The phase stability of the compositions was investigated using XRD. The phase solubility of the compositions was investigated using XRD and Raman spectroscopy (ENWAVE OPTRONICS-EZRAMAN). The granules were made by adding 3% polyvinyl alcohol as a binder. The granules were sieved and uniaxially cold pressed with a load of 6 tonnes to obtain discs with a diameter of 11 mm. The discs were decarbonised at 550 °C and then sintered between 1050 and 1175 °C for 4 hrs. The optimum sintering temperature was determined

by investigating the linear shrinkage and bulk density of the sintered pellets. The bulk density and apparent porosity were investigated using Archimedes principle (water immersion technique) and all the compositions have well sintered at 1150 °C. The structural modifications of the sintered samples have investigated using XRD and its Rietveld refinement. The prepared ceramic samples were polarized at room temperature under 35 kV/cm in silicon oil for 20 minutes. The piezoelectric coefficients d_{33} of the samples were measured using a quasi-static piezoelectric d_{33} -meter (YE2730A, China). The impedance (Z) and phase (θ) versus frequency with steps in the range 100 Hz to 1 MHz were measured using Hioki 3532 impedance-phase gain analyser. The resonant and anti-resonant frequencies for the planar vibration modes used to calculate the planar coupling coefficient (K_p) mechanical quality factor (Q_m) and the frequency constant (N_p) by the following equations:

$$K_p = \left[\frac{0.395f_r}{(f_a - f_r) + 0.574} \right]^{\frac{1}{2}} \quad (1)$$

$$Q_m = f_a^2 [2\pi R_f C f_r (f_a^2 - f_r^2)]^{-1} \quad (2)$$

$$N_p = \left(\frac{\pi d}{3.4} \right) f_r \quad (3)$$

where f_r and f_a are resonant and anti-resonant frequencies, R_f , C and d are resonant impedance, electrical capacitance and diameter of the pellet respectively.

Result and Discussion

X-Ray diffraction study

The X-ray diffraction patterns of the (1-x)BNT-(x)BZT ceramics for all compositions are shown in the Fig 1, indicating the samples have pure single phase perovskite structure with no trace of non-stoichiometry induced second phase and BZT has diffused into the lattice to form a solid-solution. As the BZT fraction in

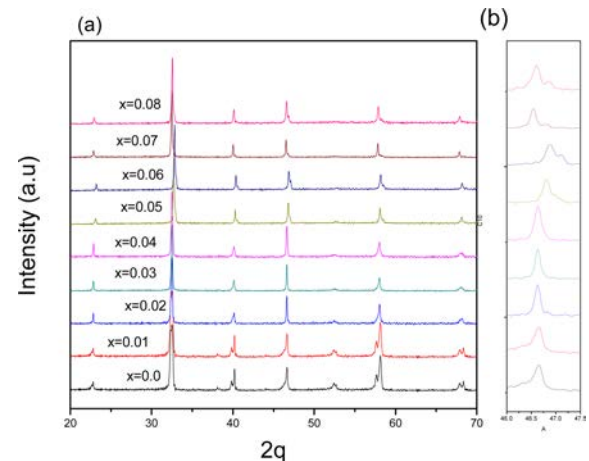


Fig. 1. X-Ray diffraction pattern of (1-x)(Bi_{0.5}Na_{0.5})TiO₃-xBa(Zr_{0.25}Ti_{0.75})O₃ ceramics (a) 20-70 ° (b) 46-48 °.

Table 1. Rietveld refinement results and atomic coordinates of 0.95(Bi_{0.5}Na_{0.5})TiO₃-0.05Ba(Zr_{0.25}Ti_{0.75})O₃ ceramics (MPB region).

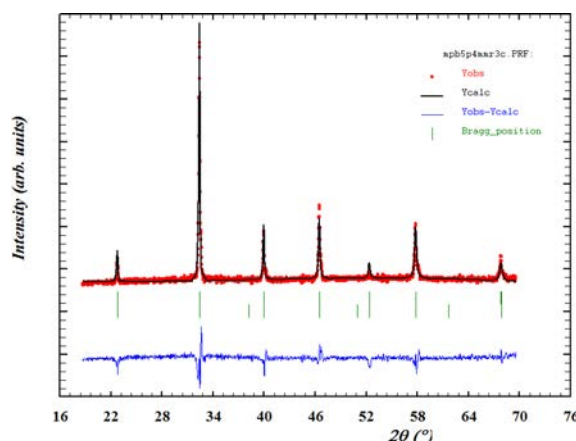
Phase	Atom	x	y	z	Biso
Rhomb. (R3c)	Bi	0	0	0.2903(13)	0.3840(18)
	Ba	0	0	0.2903(13)	0.3840(18)
	Na	0	0	0.2903(13)	0.3840(18)
	Ti	0	0	0.0177(14)	0.2840(19)
	O1	0.1596(15)	0.3297(16)	0.8866(17)	0.9734(23)
Tetra. (P4mm)	Bi	0	0	0	0.3201(16)
	Ba	0	0	0	0.3201(16)
	Na	0	0	0	0.3201(16)
	Ti	0.5	0.5	0.5356	0.2485(17)
	O1	0.5	0.5	-0.10931	0.5447(18)
	O2	0.5	0	0.41957	0.0374(19)

Table 2. Refinement results (phase percentage, cell parameter and cell volume) of the crystal structure of 0.95(Bi_{0.5}Na_{0.5})TiO₃-0.05Ba(Zr_{0.25}Ti_{0.75})O₃ ceramics.

x	Crystal system	Space group	Phase	Lattice parameters		Cell volume (Å ³)
				a = b (Å)	c (Å)	
0.07	Rhomb	R3c	55.3%	5.5202(3)	13.5229(5)	357.2(8)
	Tetra.	P4 mm	44.7%	3.9053(4)	3.9015(2)	59.5 (7)

the solid-solution increases, the (1 1 0) peaks of these BNT-BZT ceramics shift monotonically to lower 2θ angle, suggesting a consecutive increase in lattice parameter and cell volume as a function of the BZT fraction due to large radius of Ba²⁺ (1.61 Å) as compared with (Bi_{0.5}Na_{0.5})²⁺ (~ 1.40 Å). The X-ray diffraction patterns of these ceramics also demonstrate the co-existence of two phases, with increasing BZT fraction. Only the (2 0 0) peak is observed in the diffraction patterns for BNT-BZT (x ≤ 0.04) ceramics, indicating that there is only a rhombohedral structure. However, (2 0 0) and (0 0 2) peaks observed in the diffraction patterns for BNT-BZT (x = 0.08) ceramics reveal the existence of its tetragonal structure. At x = 0.05 the peak at around 47° is slightly asymmetrical, featured with slightly splitting of the (2 0 0) and (0 0 2) peaks. The more BZT content leads to the wider separation between (2 0 0) and (0 0 2) peaks, indicating the increasing tetragonality of the lattice. Therefore, it can be suggested that the morphotropic phase boundary (MPB) of (1-x)BNT-xBZT lies in the composition x = 0.05 at room temperature, where rhombohedral (R3c) and tetragonal (P4 mm) phases co-exists. Table 1 and Table 2 summarize the Rietveld refinement result carried out in the MPB composition of (1-x)BNT-xBZT solid-solutions, where the setting parameters of R3c were referred to Corker *et al.* [42] and those of P4 mm were set according to the crystallographic limitation of its space group.

Replacing the refined phase by the coexisting rhombohedral and tetragonal phases resulted in a good fitting between the observed intensities and the calculated intensities of 0.95(Bi_{0.5}Na_{0.5})TiO₃-0.05Ba(Zr_{0.25}Ti_{0.75})O₃ ceramic, as shown in Fig. 2 where the final R factor (R_p) and weighted R-factor (R_{wp}) and χ²



(The reliability factors are R_p = 16.3%, R_{wp} = 15.8%, χ² = 2.22, R_{exp} = 10.6% and R_{Bragg} = 9.8%)

Fig. 2. Rietveld refinement plots of 0.95(Bi_{0.5}Na_{0.5})TiO₃-0.05Ba(Zr_{0.25}Ti_{0.75})O₃ ceramic (MPB region).

value are 16.3%, 15.8%, and 2.22, respectively. The result indicates that 0.95BNT-0.05BZT is composed of 55.3% rhombohedral phase and 44.7% tetragonal phase, so that 0.95BNT-0.05BZT is confirmed to be an MPB composition. Also, the results obtained from the Rietveld refinement method, shown a good agreement between to the XRD patterns experimentally measured and theoretical line profile of (1-x)BNT-xBZT ceramic solid-solutions with BNT and BZT Rietveld refinement pattern.

Raman scattering study

Raman spectroscopy represents another local probe to study NBT-x%BT [43,44]. Previously reported, BNT has rhombohedral symmetry with space group R3c (C_{6v}) and BZT has cubic symmetry with space

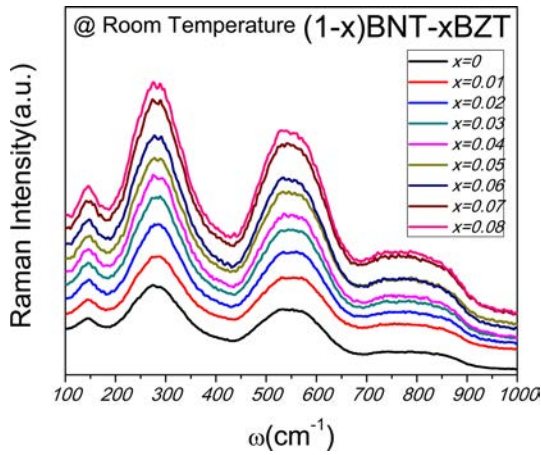


Fig. 3. Room temperature Raman spectra of $(1-x)(\text{Bi}_{0.5}\text{Na}_{0.5})\text{TiO}_3-x\text{Ba}(\text{Zr}_{0.25}\text{Ti}_{0.75})\text{O}_3$ ceramic.

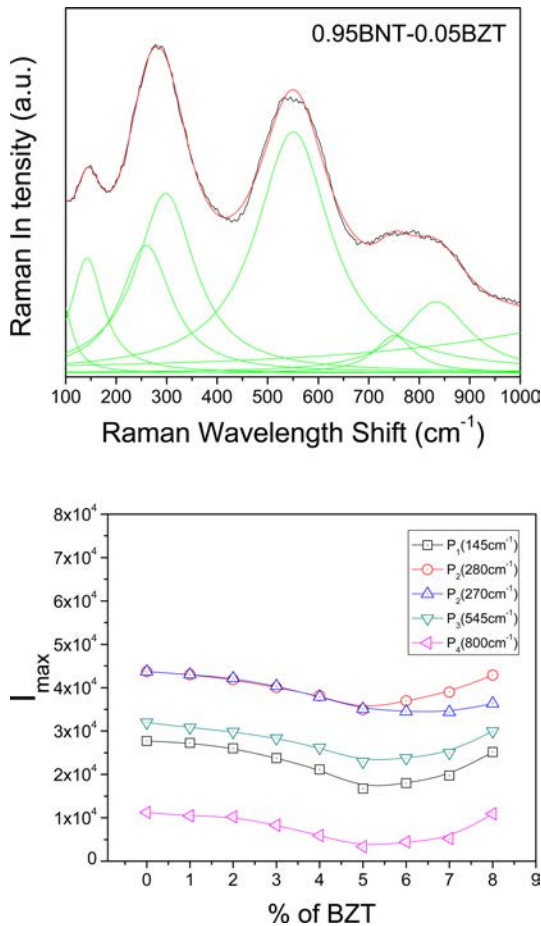


Fig. 4. (a) Fitting of the Raman spectra of $0.95(\text{Bi}_{0.5}\text{Na}_{0.5})\text{TiO}_3-0.05\text{Ba}(\text{Zr}_{0.25}\text{Ti}_{0.75})\text{O}_3$ ceramic with Lorentzian line shape (b) Variation of intensity of different modes in the Raman spectra versus BZT concentration.

group $\text{Pm}\bar{3}\text{m} (\text{O}_h^1)$ at room temperature. As far as BZT is concerned, in the cubic relaxor ferroelectric phase of the O_h^1 point group, each of the T_{1u} modes splits into a double degenerate E mode and non-degenerate A_1 mode while the T_{2u} silent mode splits into B_1+E modes. Furthermore the existence of long-range electrostatic

forces in the cubic ferroelectric phase split each of the A_1 and E modes into longitudinal and transverse modes. However, in the present case most of the analysis has been done with respect to the rhombohedral symmetry of BNT. Prior experimental investigations have shown that these peaks are broad and cannot all be resolved from each other but can be categorized into those pertaining to one of three frequency ranges [43, 44]. These are: (1) a low wave number range of 100-200 cm^{-1} which is believed to be related to Na-O vibrations; (2) a mid wave number range of 200-400 cm^{-1} which is believed to be related to Ti-O vibrations; and (3) a high wave number range of 400-800 cm^{-1} which is believed to be related to oxygen octahedral vibrations and rotations.

Fig. 3 represents the Raman spectroscopy study of $(1-x)(\text{Bi}_{0.5}\text{Na}_{0.5})\text{TiO}_3-x\text{Ba}(\text{Zr}_{0.25}\text{Ti}_{0.75})\text{O}_3$ ceramics with $0 \leq x \leq 0.08$. In BNT, rhombohedral structure with space group $\text{R}\bar{3}\text{c} (\text{Z} = 2)$ and two clusters units it is possible to observed 13 Raman-active mode, which can be represented as $(\Gamma_{\text{Raman}} = 7\text{A}_1 + 6\text{E})$ [45]. However, it is possible to detect only five Raman-active modes observed in the range from 100 to 1000 cm^{-1} in agreement with the works reported by the Rout *et al.* [46] and Eerd *et al.* [47]. Due to the disorder into-A site related to distorted octahedral $[\text{BiO}_6]$ and $[\text{NaO}_6]$ clusters, these BNT ceramics with rhombohedral structure presents 13 Raman-active modes by the following representation: $(\Gamma_{\text{Raman}} = 4\text{A}_1 + 9\text{E})$ that have been seen analyzed and reported by the Petzelt *et al.* [48]. In Fig. 3, the Raman peaks of BNT and BNT-BZT solid-solutions are relatively broad, which can be caused by the distorted octahedral $[\text{BiO}_6]$ and $[\text{NaO}_6]$ clusters or disorder in A-site of rhombohedral structure. Also this behaviour can be provoked possible due to presence of the disorder structural or distorted octahedral $[\text{TiO}_6]$ clusters at short-range in both (rhombohedral and cubic) lattices. The first Raman-active $\text{A}_1(\text{TO}_1)$ mode at around (146 cm^{-1}) is related to network modifiers or distorted octahedral $[\text{BiO}_6]$ and $[\text{NaO}_6]$ clusters. The second Raman-active $\text{E}(\text{TO}_2)$ mode can be deconvoluted in three Raman peaks in the regions of 279 cm^{-1} . This mode is assigned at stretching arising from the bonds due the presence of octahedral $[\text{TiO}_6]$ clusters at short-range. The mode shows anomaly at $x = 0.05$ and starts splitting into two bands that shift apart from each other with further increase in BZT content. The splitting of the B peak(s) at room temperature with increasing x for NBT-x%BT reveals a change in symmetry (relative to NBT), to a structure whose irreducible representation has a higher number of Raman active modes. The third Raman-active (LO_2) mode with low intensity is related to short-range electrostatic forces associated with the lattice ionicity [49]. According to Dobal *et al.* [50], the (TO_3) modes situated at around 542 cm^{-1} is ascribed to the $(\leftarrow \text{O} \leftarrow \text{Ti} \rightarrow \text{O} \rightarrow)$ stretching symmetric vibrations of the octahedral $[\text{TiO}_6]$ clusters. This mode is common in

materials with type-perovskite structure. However the spectral signature of bands shows a change at $x = 0.05$ and separate in to two distinct bands at $x = 0.07$. At higher composition (0.08) the band appears to split into three weak Raman bands, similar observations are found in BaTiO_3 and PbTiO_3 compounds in earlier reports [51, 52]. Finally, the (LO3) mode found at 812 cm^{-1} is due to presence of the sites within the rhombohedral lattice pre containing octahedral distorted $[\text{TiO}_6]$ clusters [53]. These modes are classified into longitudinal (LO) and transverse (TO) components because of the electronic structure with polar character of lattice.

Fig. 4 (a) Room temperature Raman spectrum of 0.95BNT-0.05BZT (MPB, composition) ceramics & (b) Variation of the maximum intensity of different modes in the Raman spectra with % of BZT concentration. In Fig.4(a) fitted by Lorentzian area function for MPB composition of BNT-BZT solid-solutions, which clearly shows the overlapping of Raman bands due to anharmonicity in lattice during molecular vibrations. In Fig. 4 (b) shows the minimum intensity occurs at $x = 0.05$ due to the maximum strain in the lattice and existence of MPB composition, which is well aligned with the studies of XRD phase analysis. The dramatically enhanced intensity of the Raman bands when the x value is increased further, suggests the occurrence of a long range ordering of the corresponding phases involved [54-56].

Microstructural Study:

Fig. 5 shows the SEM images of natural surface for $(1-x)\text{BNT}(x)\text{BZT}$ ceramics sintered at $1150\text{ }^\circ\text{C}$ for 4 hours. The pure BNT sample presents rectangular grain morphology while the BZT addition changes the grain shape to spherical shape. All sample surface grains present regular geometry with compact structure. BNT disk appears to be poly-dispersed in both size and shape due to inhomogeneous grain growth. On the contrary, the addition of BZT results in the inhibition of grain growth, so the crystals of the BNT-BZT appear to be more uniform in both size and shape. Several possible mechanisms were reported to show how the liquid-phase could homogenize the microstructure [57]. The first possibility is that the liquid-phase assists rearrangement of the matrix particles at the inclusion/matrix interface into a more efficient packing configuration. The second possibility is that the liquid-phase goes into the polycrystalline inclusions by capillary action to break them up and homogenize the microstructure. It can also be seen that the grain size reduces with increase in BZT content in the compositions up to $x = 0.04$. The reason may be that Ba^{2+} abounds in crystal boundary, which prevents the ion from migrating and restrains the growing of grains. The SEM observation confirms that the $(1-x)\text{BNT}(x)\text{BZT}$ ceramics are densely sintered and all compositions have high density density between 5.67

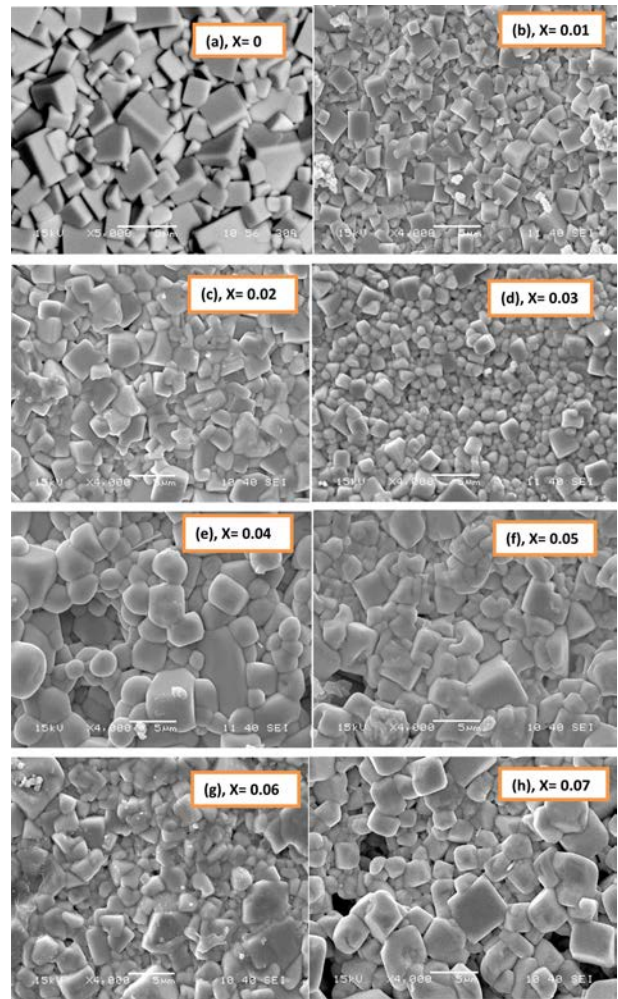


Fig. 5. (a-h) SEM micrographs of $(1-x)(\text{Bi}_{0.5}\text{Na}_{0.5})\text{TiO}_3-x\text{Ba}(\text{Zr}_{0.25}\text{Ti}_{0.75})\text{O}_3$ ceramic.

and 5.83 g/cm^3 , about more than 96% of the theoretical density.

Piezoelectric and electromechanical study:

Fig. 6 shows the frequency impedance/spectra of the BNT-BZT solid solution at its MPB composition. Fig. 7 (a) presents the piezoelectric and electromechanical properties of $(1-x)\text{BNT}(x)\text{BZT}$ ceramics. The piezoelectric constant d_{33} and electromechanical coupling factor k_p display a similar variation, enhancing with the increasing of x through a maximum value in a composition near the MPB and then tending to decrease. A strong compositional dependence of d_{33} and K_p was observed. The sample with $x = 0.05$, which is close to the MPB as demonstrated by the XRD patterns in Fig. 1, displays the best value of 131 pC/N and the electromechanical coupling factor k_p reaches to the maximum value of 23%. It is evident that the MPB between the orthorhombic and tetragonal perovskite phases plays an important role in enhancing the piezoelectric properties. The instability in the domain structure might facilitate the polarization switching and thus improve the piezoelectricity. In the MPB region, the

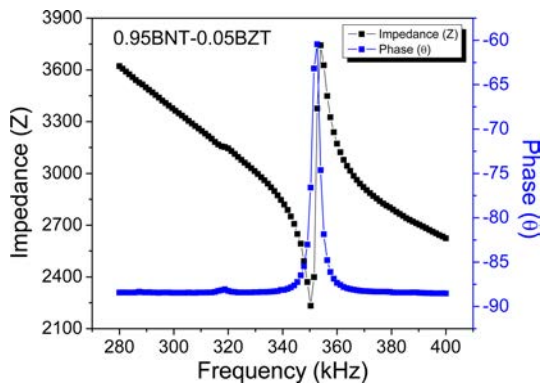


Fig. 6. The frequency vs. impedance/phase spectrum of 0.95BNT-0.05BZT ceramic (MPB composition).

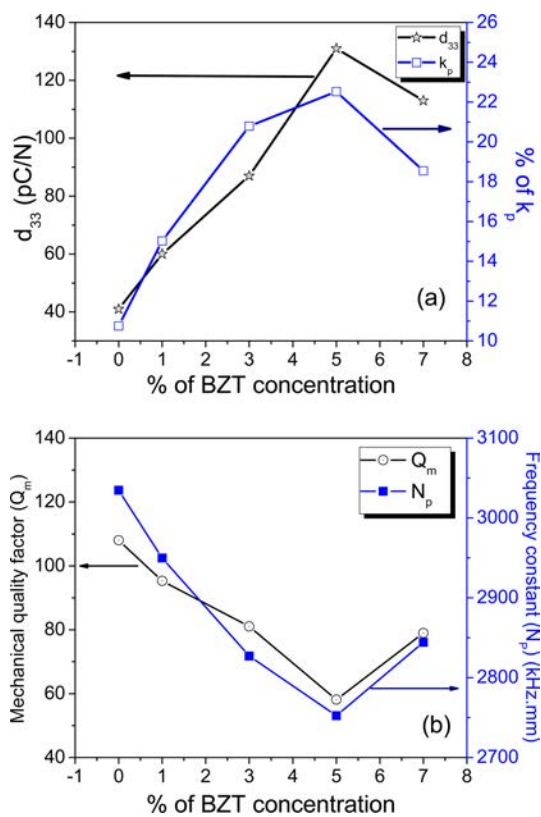


Fig. 7. (a) piezoelectric co-efficient (d_{33}) and electromechanical coupling factor (k_p) and (b) Mechanical quality factor (Q_m) and frequency constant (N_p) of BNT-BZT ceramics with % of BZT concentration.

polarization vector can easily switch (upon application of a small field) between all the allowed polarization orientations, and hence enhances the piezoelectric coefficient [58].

Mechanical quality factor (Q_m) is an important parameter for piezoelectric applications. Ceramics with high Q_m are electrically “hard” to switch, i.e., more difficult to pole, but the poled remnant state is more stable during mechanical and thermal loading, making them ideal for actuator applications. Composition dependences of Q_m and frequency constant (N_p) of BNT-BZT ceramics are shown in Fig. 7. From Fig. 7(b),

it can be seen that the mechanical quality factor Q_m of the specimens decreases with increasing x , reaches the minimum value at $x = 0.05$ and then shows a slight increase with more values of x . A tendency of frequency constant N_p of the specimens similar to the Q_m can be seen, which confirms the MPB at $x = 0.05$. The changes of Q_m and $\tan \delta$ with structures are believed to be associated with the domain wall motion. Increasing tetragonal distortion induces strain in the crystal lattice, which would hinder the domain wall mobility and stabilize the domain configuration during the application of an external field, and therefore, Q_m increases and $\tan \delta$ decreases with increasing BZT content. From the above electromechanical properties of the solid solution BNT-BZT systems, it can be concluded that the good piezoelectric and electromechanical properties lie in near MPB composition range similar to other systems. It is attributed to an increase in the number of possible spontaneous polarization direction for the compositions near the MPB due to the coexistence of rhombohedral and cubic phases. This is also explained by having equivalent energy for the coexistence of rhombohedral and cubic phases can be transformed each other in poling process, which enhance the piezoelectric and electromechanical activities.

Conclusions

$(\text{Bi}_{0.5}\text{Na}_{0.5})\text{TiO}_3\text{-Ba}(\text{Zr}_{0.25}\text{Ti}_{0.75})\text{O}_3$ solid-solution ceramics were successfully synthesized by a conventional solid state reaction rout. X-ray diffraction analysis has shown that all the compositions are characterised by a pure perovskite structure without any parasite phase. It is observed that the addition of BZT allows a phase transformation from the rhombohedral phase to the tetragonal phase. By the Rietveld refinement analysis, the MPB composition is found at $x = 0.05$ which presents 55.3% of the rhombohedral phase and 44.7% of the tetragonal phase. Also, Raman spectroscopy study has been confirmed the existence of morphotropic phase boundary (MPB) at $x = 0.05$ composition. The piezoelectric measurement shows piezoelectric coefficient increases with an increase in BZT content and optimum value at $x = 0.05$. Also electromechanical study shows optimum results at $x = 0.05$ confirming the MPB composition. Both the structural and electrical properties show that the solid solution has a MPB around $x = 0.05$ which is expected to be a new candidate for lead-free piezoelectric material.

References

1. G.O. Jones, P.A. Thomas, *Acta Crystallogr. Sect. B* 56 426 (2000)
2. A. Herabut and A. Safari, *J. Am. Ceram. Soc.* 80, 2954 (1997)
3. H. Nagata, T. Shinya, Y. Hiruma, T. Takenaka, I. Sakaguchi, and H. Haneda, *Ceram. Trans.* 167, 213 (2005).

4. G. A. Smolenskii, V. A. Isupov, A. I. Agranovskaya, and N. N. Krainik, *Sov. Phys. Solid State* 2, 2651 (1961).
5. J. A. Zvirgzds, P. P. Kapostis, and J. V. Zvirgzde, *Ferroelectrics* 40, 75 (1982)
6. G. O. Jones and P. A. Thomas, *Acta Crystallogr., Sect. B: Struct. Sci.* 56, 426 (2000).
7. G. O. Jones and P. A. Thomas, *Acta Crystallogr., Sect. B: Struct. Sci.* 58, 168 (2002).
8. J. Kreisel, A.M. Glazer, P. Bouvier, G. Lucazeau, *Phys. Rev.*, B 63, 174106 (2001).
9. O. Elkechai, P. Marchet, P. Thomas, M. Manier, J.P. Mercurio, *J. Mater. Chem.* 7, 91 (1997).
10. Y. Hiruma, H. Nagata, T. Takenaka, *J Appl Phys* 104, 124106 (2008).
11. G.A. Smolenskii, V.A. Isupov, I.A. Agranovskaya, N.N. Krainik, *Sov Phys Solid State* 2, 2651 (1961).
12. Y. Hiruma, H. Nagata, and T. Takenaka, *Jpn. J. Appl. Phys.*, Part 1 45, 7409 (2006).
13. Y. Hiruma, K. Yoshii, H. Nagata, and T. Takenaka, *Ferroelectrics* 346, 114 (2007).
14. Y. Hiruma, Y. Watanabe, H. Nagata, and T. Takenaka, *Key Eng. Mater.* 350, 93 (2007).
15. Y. Hiruma, K. Yoshii, H. Nagata, and T. Takenaka, *J. Appl. Phys.* 103, 084121 (2008).
16. Y. Watanabe, Y. Hiruma, H. Nagata, and T. Takenaka, *Key Eng. Mater.* 388, 229 (2008).
17. Y. Hiruma, H. Nagata, and T. Takenaka, *IEEE Trans. Ultrason. Ferroelectr. Freq. Control* 54, 2493 (2007).
18. T. Takenaka, K. Maruyama, and K. Sakata, *Jpn. J. Appl. Phys.*, Part 1 30, 2236 (1991).
19. Y.-M. Chiang, G. W. Farrey, and A. N. Soukhojak, *Appl. Phys. Lett.* 73, 3683 (1998).
20. A. Sasaki, T. Chiba, Y. Mamiyal, and E. Otsuki, *Jpn. J. Appl. Phys.*, Part 1 38, 5564 (1999).
21. S. A. Sheets, A. N. Soukhojak, N. Ohashi, and Y.-M. Chiang, *J. Appl. Phys.* 90, 5287 (2001).
22. B. J. Chu, D. R. Chen, G. R. Li, and Q. R. Yin, *J. Eur. Ceram. Soc.* 22, 2115 (2002).
23. H. Nagata, M. Yoshida, Y. Makiuchi, and T. Takenaka, *Jpn. J. Appl. Phys.*, Part 1 42, 7401 (2003).
24. X. X. Wang, X. G. Tang, and H. L. W. Chan, *Appl. Phys. Lett.* 85, 91 (2004).
25. Y. Hiruma, Y. Makiuchi, R. Aoyagi, H. Nagata, and T. Takenaka, *Ceram. Trans.* 174, 139 (2005).
26. L. Wu, D.-Q. Xiao, D.-M. Lin, J.-G. Zhu, and P. Yu, *Jpn. J. Appl. Phys.*, Part 1 44, 8515 (2005).
27. L. Wu, D. Xiao, D. Lin, J. Zhu, P. Yu, and X. Li, *Jpn. J. Appl. Phys.*, Part 1 46, 7382 (2007).
28. D. Lin, D. Xiao, J. Zhu, and P. Yu, *Appl. Phys. Lett.* 88, 062901 (2006).
29. D. Lin, K. W. Kwok, and H. W. L. Chan, *J. Phys. D* 40, 5344 (2007).
30. S. Zhang, T. R. Shrout, H. Nagata, Y. Hiruma, and T. Takenaka, *IEEE Trans. Ultrason. Ferroelectr. Freq. Control* 54, 910 (2007).
31. Y.-R. Zhang, J.-F. Li, B.-P. Zhang, and C.-E. Peng, *J. Appl. Phys.* 103, 074109 (2008).
32. T. Takenaka, K.I. Maruyama, K. Sakata, *Jpn. J. Appl. Phys.* 30, 2236 (1991).
33. Z. Yu, C. Ang, R. Guo, A.S. Bhalla, *J. Appl. Phys.* 92, 1489 (2002).
34. N. Nanakorn, P. Jalupoom, N. Vaneesorn, A. Thanaboonmbut, *Ceram. Int.* 34, 779 (2008).
35. T. Maiti, R. Guo, A.S. Bhalla, *Appl. Phys. Lett.* 90, 182801 (2007).
36. Y.Q. Yao, T.Y. Tseng, C.C. Chou, H.H.D. Chen, *J. Appl. Phys.* 102, 094102 (2007).
37. C.C. Jin, F.F. Wang, Q.R. Yao, Y.X. Tang, T. Wang, W.Z. Shi, *Cera. Inter.* 40 6143 (2014).
38. P. Chune, L. T. Jing-Feng, G. Wen, *Materials Letters* 59, 1576 (2005).
39. Z. Yu, C. Ang, R.Y. Guo, A.S. Bhalla, *J. Appl. Phys.* 92, 1489 (2002).
40. D. Peng, L. Luo, W. Li, Yueping Zhang, Hongbing Chen, *Jour Alloys and Comp* 559, 92 (2013).
41. T. Badapanda, S.K. Rout, L.S. Cavalcante, J.C. Sczancoski, S. Panigrahi, E. Longo, M.S. Li, *J. Phys. D: Appl. Phys.* 42, 175414 (2009).
42. D.L. Corker, A.M. Glazer, R.W. Whatmore, A. Stallard, F. Rauth, *J Phys: Condens Matter* 10, 6251 (1998).
43. M. S. Zhang and J. F. Scott, *Phys. Rev. B* 34, 1880 (1986).
44. I. G. Sinii, T. A. Smirnova, and T. V. Kruzina, *Fiz. Tverd. Tela* 33, 110 (1991).
45. X. Wang, X.G. Tang, H.L.W. Chan, *Appl Phys Lett* 85, 91 (2004).
46. G.F. Fan, W.Z. Lu, X.H. Wang, F. Liang, *Appl Phys Lett* 91, 202908 (2007).
47. S.T. Zhang, F. Yan, B. Yang, W.W. Cao, *Appl Phys Lett* 97, 122901 (2010).
48. Y. Hosono, K. Harada, Y. Yamashita, *Jpn J Appl Phys* 40, 5722 (2001).
49. B.J. Chu, D.R. Chen, G.R. Li, Q.R. Yin, *J Eur Ceram Soc* 22, 2115 (2002).
50. D. Rout, K.S. Moon, V.S. Rao, S.J. L. Kang, *J Cerm Soc of Japan* (2009) 117 [7]: 797-800.
51. K. Pengpat, S. Hanphimol, S. Eitssayeam, U. Intatha, G. Rujijanagul, T. Tunkasiri, *J. Electroceram* 16, 301 (2006).
52. W. Jo, J.E. Daniels, J.L. Jones, X. Tan, P.A. Thomas, D. Damjanovic, J. Rödel, *J Appl Phys* 109, 014110 (2011).
53. I.G. Siny, E. Husson, J.M. Beny, S.G. Lushnikov, E.A. Rogacheva, P.P. Symikov, *Ferroelectrics* 248, 57 (2000).
54. J. Kreisel, A.M. Glazer, G. Jones, P.A. Thomas, L. Abilo, G. Lucazeau, *J Phys: Condens Matter* 12, 3267 (2000).
55. S. Trujillo, J. Kreisel, Q. Jiang, J. H. Smith, A. P. Thomas, P. Bouvier, F. Weiss, *J Phys: Condens Matter* 17, 6587 (2005).
56. J. Wang, Z. Zhou, J. Xue, *Acta Materials* (2006) 54:1691.
57. R.M. German, *Liquid Phase Sintering*, Plenum Press, New York, 1985.
58. Chune Peng, Jing-Feng Li, T. Wen Gong, *Materials Letters* 59, 1576 (2005).